Solid State Communications 151 (2011) 965–970

Contents lists available at ScienceDirect

Solid State Communications

journal homepage: www.elsevier.com/locate/ssc

Calculation of thermodynamic properties of Ni nanoclusters via selected equations of state based on molecular dynamics simulations

Hamed Akbarzadeh [a,*], Hadi Abroshan [a], Farid Taherkhani [b], Gholam Abbas Parsafar [a,c,**]

[a] Department of Chemistry, Sharif University of Technology, Tehran, 11365-9516, Iran

[b] Department of Chemistry, Science College, Razi University, Kermanshah, Iran

[c] Institute for nanoscience and nanotechnology, Sharif University of Technology, Tehran, 11365-9516, Iran

ARTICLE INFO

Article history:
Received 8 October 2010
Received in revised form
5 February 2011
Accepted 11 May 2011
by S. Scandolo
Available online 17 May 2011

Keywords:
A. Nickel nanocluster
B. Molecular dynamics
C. Equation of state
C. Bulk modulus

ABSTRACT

We present an approach for constant-pressure molecular dynamics simulations. This approach is especially designed for finite systems, for which no periodic boundary condition applies. A molecular dynamics (MD) simulation for Ni nanoclusters is used to calculate their pressure–volume–temperature (p–v–T) data for the temperature range 200 K $\leq T \leq$ 400 K, and pressures up to 600 kbar. Isothermal sets of p–v–T data were generated by the simulation; each set was fitted by three equations of state (EoSs): Linear Isotherm Regularity-II (LIRII), Birch–Murnaghan (BM), and EOS III. It is found that the MD data are satisfactorily reproduced by the EoSs with reasonable precision. Some features of the EoSs criteria, such as the temperature dependences of the coefficients, the isothermal bulk modulus and its pressure derivative at the zero-pressure limit, and isobaric thermal expansion for Ni nanoclusters, are investigated. We have found that same EoSs are valid for both bulk Ni and Ni nanoclusters, but with different values of the parameters, which depend on the cluster size and temperature. An increase in bulk modulus with decrease of cluster size can be observed. Also, an increase in isobaric expansion coefficient with decrease of cluster size has been found.

© 2011 Elsevier Ltd. All rights reserved.

1. Introduction

Nickel is a transition ferromagnetic 3d metal that is widely used as a catalyst [1–3]. Xiaogang et al. [4] studied the equation of state (EoS) of nanosize and bulk nickel powders up to 50 GPa, and suggested that nanonickel is more compressible than bulk nickel, whereas Chen et al. [5] measured the compressibility of nanocrystalline nickel particles with size of 20 nm under quasihydrostatic pressures up to 55 GPa and reported that the bulk modulus did not vary with the particle size when compared to the theoretical results [6]. Also, Rekhi et al. [7] and Raju et al. [8] measured the compressibility of nanosized nickel particles of size 20 nm and 62 nm, respectively, under pressures up to 61.5 GPa and 56 GPa, respectively, and reported that the bulk modulus varies with the particle size. The grain-size dependence of the bulk modulus of nanocrystalline Ni has recently been investigated using molecular dynamics (MD) simulation [9].

Three methods to apply pressure to nanosystems (using an auxiliary pressure transmitting medium) have been reported.

1. Martonak et al. [10–13] immersed a cluster into a model classical liquid, described by a soft-sphere potential, which acts as a pressure reservoir. The pressure is varied by tuning the parameter of the liquid potential.

2. The nanocrystals are embedded in a hydrostatic pressure medium for which a Lennard-Jones (LJ) liquid was chosen [14–16].

3. Grunwald and Dellago [17] used an ideal gas flow through a surface to apply pressure on CdSe nanoparticles in their computer simulations.

Also, Sun and Gong [18] presented a method for constant-pressure molecular dynamics simulation which is parameter free for finite systems.

We have used a variation of the methodology proposed by Grunwald and Dellago, consisting of filling the simulation box with idealized particles that interact with the Ni atoms via a soft core repulsive potential (ideal gas). One of the variations proposed consists of assuming that some of the gas atoms interact with the Ni atoms via a Lennard-Jones potential, thus introducing an attractive component as well. This is justified as a means to improve convergence in the calculated pressure. Another variation consists of fixing the number of gas atoms, while, in the Grunwald–Dellago method, they allow for the gas particles to enter or leave the simulation box through a surface. Our approach allows controlling the pressure. (Note that having a nanocluster

* Corresponding author. Tel.: +98 21 66165355; fax: +98 21 66005718.
** Corresponding author.
E-mail addresses: akbarzadehhamed@yahoo.com (H. Akbarzadeh), parsafar@sharif.edu (G.A. Parsafar).

0038-1098/$ – see front matter © 2011 Elsevier Ltd. All rights reserved.
doi:10.1016/j.ssc.2011.05.011

surrounded by ideal particles, only interacting via repulsive forces, is expected to generate a pressure gradient.)

The purpose of the present work is to generate realistic pressure–volume–temperature (p–v–T) isotherm simulation data for Ni nanoclusters and thereby to investigate the precision of some equations of state (EoSs) and calculate some of their thermodynamic properties.

2. Molecular dynamics simulation

In our simulations, the pressure medium consists of particles that do not interact with each other, but do interact with the Ni atoms in the crystal via a soft-sphere potential of the form

$$U(r) = \varepsilon \left(\frac{\sigma}{r}\right)^{12}, \tag{1}$$

where r denotes the distance between two particles, σ the interaction range, and ε the interaction strength [17]. We may use argon (or any other ideal gas) as the pressure medium in these simulations. However, if one merely takes the interaction potential of Eq. (1) between each Ar atom and the nanocluster, the desired pressure would not be achieved. To overcome this problem, we may assume that a small number of argon atoms interact with the nanocluster as follows, instead of Eq. (1).

$$V_{LJ} = 4\varepsilon \left[\left(\frac{\sigma}{r}\right)^{12} - \left(\frac{\sigma}{r}\right)^{6}\right]. \tag{2}$$

Note that, unlike Eq. (1), in which the potential parameters are arbitrary, the Lennard-Jones potential parameters for nickel–argon ($\varepsilon = 8.642$ kJ/mol, $\sigma = 2.84$ Å [9,19]) are used in Eq. (2). The fraction of Ar atoms that interact through Eq. (2) may be found by trial and error, in such a way that leads to the desired pressure. To obtain the equilibrium position with the desired pressure, the potential parameters have significant influences on the pressure. However, by fixing the potential parameters, the pressure value changes by variation of the number of particles. For example, when our goal is to achieve a pressure equal to 1 bar, considering the repulsive potential alone, we cannot exactly reach this pressure. Therefore, we consider a very small fraction of the gas atoms interacting through Eq. (2). This very small fraction is determined by trial and error. The system at low temperatures can be developed by considering the potential parameters between liquid Ar and the nanoclusters. Incidentally there are other ways to apply pressure without the pressure transmitting medium, as described in [18,20,21] and the references therein, depending on the definition of the volume.

We have used Quantum Sutton–Chen (QSC) potential for the Ni–Ni interactions. The QSC parameters for Ni are listed in Table 1 [22,23].

The MD simulations are carried out in an *NpT* ensemble with periodic boundary conditions, for the system including the nanocluster and argon gas. The temperature and pressure are controlled by a Nose–Hoover thermostat and barostat [24]. In order to have an isotropic constant pressure on the cluster, the number of gas particles and the gas volume should be much larger than those of the cluster. In these simulations, we have used 32 000 gas particles. The equations of motion are integrated using the Verlet Leapfrog algorithm [9] with a time step of 0.001 ps. The system was equilibrated for 500 ps, the averages were computed over the following 1 ns. The cutoff length is chosen to be 8 Å in the simulations.

In the present study, we have used the DL-POLY-2.20 program [25]. Also, the results for bulk Ni were obtained from different MD simulations for some isotherms. The experimental [26,27] and calculated densities for solid Ni at 300 K and zero pressure are, respectively, 151.805 and 147.279 mol/L. The agreement between the two values is within 2.98%.

Table 1
Potential parameters used in MD simulation for the Ni nanoclusters.

	n	m	ε (eV)	c	a (Å)
QSC	10	5	7.3767×10^{-3}	84.745	3.5157

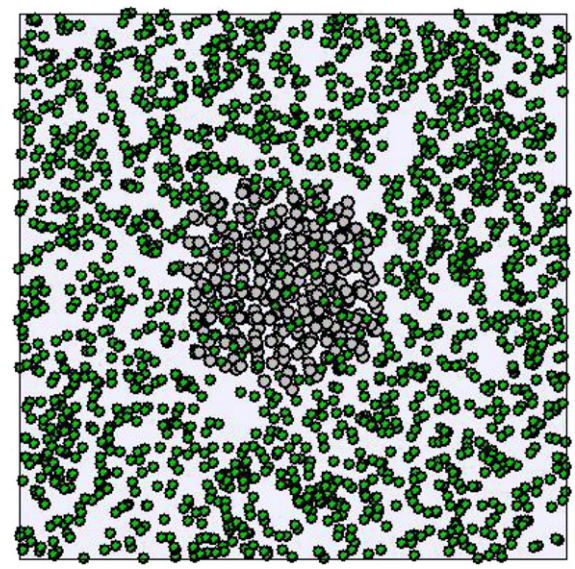

Fig. 1. Snapshot of a Ni nanocluster with 336 atoms immersed in an ideal gas pressure bath with 1 kbar pressure at 300 K.

We have removed some Ar atoms from the cube center, to replace the Ni nanocluster in the center of the ideal gas pressure bath (center of cube). Fig. 1 shows a Ni nanocluster with 336 atoms immersed in an ideal gas pressure bath with 1 kbar pressure at 300 K.

After the simulations are done, we have to define the volume of the nanocluster. The volume of the cluster was obtained using a volume definition based on a Wigner–Seitz primitive cell [18].

Simulations have been performed under different isothermal conditions (200–400 K) and for pressures up to 60 GPa for different sizes of the Ni nanocluster (with 336, 484, 736, 1004, and 1956 Ni atoms).

3. Some universal equations of state

The equations of state (EoSs) of solids play an important role in condensed matter physics and geophysics. They provide much information about the nonlinear compression of materials at high pressures, and have been widely applied in engineering and other branches of science. Most EoSs are expressed by three zero-pressure parameters: molar volume, v_0, isothermal bulk modulus, B_0, and its first isothermal pressure derivative, B_0'.

3.1. Birch–Murnaghan (BM) EoS

In terms of the so-called Birch–Murnaghan EoS [28,29], the pressure as a function of volume behaves as follows:

$$p = (3/2)B_0 \left[\left(\frac{v_0}{v}\right)^{7/3} - \left(\frac{v_0}{v}\right)^{5/3}\right] \times \left\{1 - (3/4)\left(4 - B_0'\right)\left[\left(\frac{v_0}{v}\right)^{2/3} - 1\right]\right\}, \tag{3}$$

where v and v_0 are the volume at p and zero pressure, respectively.

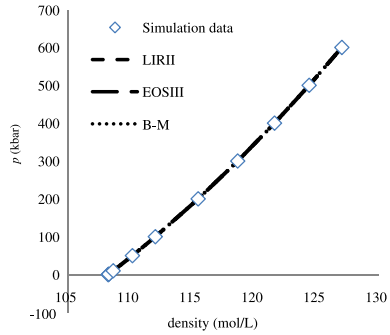

Fig. 2. Fitting three EoSs onto the simulation data of a Ni nanocluster with 336 atoms at 300 K (note that the fitting curves are superimposed on a single curve).

3.2. Linear isotherm regularity-II (LIR II)

According to the linear isotherm regularity (LIR) [30] EoS, $(Z-1)\,v^2$ is linear with respect to ρ^2 for each isotherm of a fluid.

Shokouhi et al. have extended the LIR EoS separately to two classes of solids [31], one for metallic and ionic solids and the other for the remaining solids, on the basis of the concept of the average effective pair potential. For the former materials, $(Z-1)v^2$ is linear with respect to $v = 1/\rho$, which will be referred to as LIR II (Eq. (4)) from now on, for each isotherm, and for the latter materials, the EoS is the same as that for fluids.

$$(Z-1)\,v^2 = c + d\,(1/\rho)\,, \tag{4}$$

where $Z = \frac{p}{\rho RT}$, and c and d are temperature-dependent parameters. This EOS was originally proposed for liquid metals.

3.3. Parsafar–Spohr–Patey (EoS III)

Recently, Parsafar et al. [32] have developed an EoS that gives a good description for all types of fluid, including nonpolar, polar, hydrogen-bonded, and metallic, for temperatures ranging from the triple point to the highest temperature for which experimental data are reported. For solids, the EoS is very accurate for all types considered, including covalent, molecular, metallic, and ionic systems. According to this equation, $(Z-1)v^2$ in terms of ρ may be given as

$$(Z-1)v^2 = e + \frac{f}{\rho} + g\rho^2, \tag{5}$$

where e, f, and g are temperature-dependent parameters.

4. Results and discussions

There are two ways to study the compression data: either (i) by using the exact measured values at the zero-pressure limit; then, B_0 and B_0' are used as inputs which, when error-free compression and bulk moduli data are available, can result in a perfect well-behaved EoS; or (ii) by a curve-fitting method, in which all zero-pressure values are treated as adjustable parameters and can reproduce the ideal set of zero-pressure values as inputs. Since the zero-pressure values obtained by the best fitting do not have high accuracies, we have fitted all isothermal simulation data to all EoSs mentioned in the last section. For example, as shown in Fig. 2, for 336 Ni atoms at 300 K, the simulation data are well fitted by all EoSs with a high accuracy (R^2, for each case, is 1.0).

The values of B_0 and B_0' for each isotherm of nanoclusters of different sizes are obtained from each EoS, whose parameters are

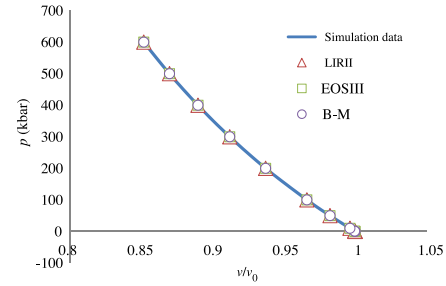

Fig. 3. Comparison of the p–v curves obtained from the three EoSs, when the zero-pressure quantities are used as inputs for a Ni nanocluster with 336 atoms at 300 K.

obtained from the fitting. The dependences of B_0 and B_0' on the parameters of EOS III are as follows:

$$B_0(T) = RT\rho_0(3e\rho_0^2 + 2f\rho_0 + 5g\rho_0^4 + 1) \tag{6}$$

$$B_0'(T) = \frac{9e\rho_0^2 + 4f\rho_0 + 25g\rho_0^4 + 1}{3e\rho_0^2 + 2f\rho_0 + 5g\rho_0^4 + 1}. \tag{7}$$

Also, the dependences of B_0 and B_0' on the parameters of LIR II are as follows:

$$B_0(T) = RT\rho_0(3c\rho_0^2 + 2d\rho_0 + 1) \tag{8}$$

$$B_0'(T) = \frac{9c\rho_0^2 + 4d\rho_0 + 1}{3c\rho_0^2 + 2d\rho_0 + 1}, \tag{9}$$

where $\rho_0 = 1/v_0$ is the cluster density at zero pressure. The calculated values of B_0 and B_0' given by the three EoSs are summarized in Table 2.

The experimental values of B_0 and B_0' ($B_0 = 1850$ kbar and $B_0' = 5$ [24], $B_0 = 1800$ kbar and $B_0' = 4$ [25]) for bulk Ni at 300 K and zero pressure are in agreement with our results (see Table 2). However, the value of B_0 given by EOS III (1854 kbar) is the closest value to experimental value reported in [24].

It is worth noting that all EoSs used in this work predict the same value for ρ_0 as that obtained from our simulations. As shown in Table 2, an increase in bulk modulus with number of particles can be observed. The hardness and yield stress of some materials increase with decreasing cluster size according to the Hall–Petch effect [33,34]. However, the reverse Hall–Petch effect, which is related to the softening of materials for very small cluster size, has also been reported [35,36]. According to our results given in Table 2, the bulk modulus of a Ni nanocluster increases when the nanocluster becomes smaller, i.e., there is a reverse Hall–Petch effect. Such behavior is expected, because of the fact that, as the cluster size reduces, proportionally more atoms are on the surface of the cluster. Since surface atoms have less binding energy, compared to the bulk atoms, with a decrease in number of particles, the compressibility is expected to decrease. A lattice with a larger binding energy needs a stronger force to be compressed by a certain amount, because the potential energy with respect to displacement of a molecule from its equilibrium position is greater. Such behavior, the reverse Hall–Petch effect, is expected to be valid so long as the geometry of the nanocluster remains unchanged. In fact, as shown in Fig. 1, the Ni nanoclusters investigated in this work are all spherical.

In the second method, we used zero-pressure simulation values as inputs and expressed the behavior of the pressure as a function of compression, v/v_0. In Fig. 3, the pressure is plotted as a function of v/v_0 for a Ni nanocluster with 336 atoms at 300 K. The three EoSs are well fitted onto the simulation data (R^2 for each fitting is 1.0).

The parameters c and d of LIR II are almost linear versus $1/T$ for the largest nanocluster, like that for bulk systems [37]. However, the deviations from linearity become significant for the smaller

Table 2
The calculated values of B_0 and B_0' obtained from the three different EoSs at given temperatures, for both nanoclusters and bulk Ni.

N	T (K)	BM B_0 (kbar)	BM B_0'	LIR II B_0 (kbar)	LIR II B_0'	EoS III B_0 (kbar)	EoS III B_0'
336	200	2651	3.91	2439	4.98	2599	4.15
484	200	2413	3.86	2178	4.99	2360	4.12
736	200	2302	3.79	2058	4.99	2249	4.08
1004	200	2231	3.71	1975	4.99	2178	4.02
1956	200	2172	3.64	1911	4.99	2117	3.97
Bulk	200	1807	3.58	1721	5.0	1799	3.97
336	250	2680	3.96	2461	4.99	2629	4.18
484	250	2451	3.90	2227	4.99	2400	4.15
736	250	2342	3.83	2109	4.99	2290	4.10
1004	250	2261	3.75	2015	4.99	2209	4.05
1956	250	2213	3.70	1961	4.99	2158	4.02
Bulk	250	1843	3.63	1812	4.99	1823	4.01
336	300	2711	4.02	2495	5.00	2660	4.23
484	300	2490	3.96	2279	4.99	2441	4.19
736	300	2384	3.89	2156	5.00	2331	4.15
1004	300	2302	3.81	2064	4.99	2250	4.09
1956	300	2240	3.74	1990	4.99	2189	4.04
Bulk	300	1889	3.69	1841	5.02	1854	4.03
336	350	2752	4.07	2543	5.00	2700	4.27
484	350	2542	4.00	2326	5.00	2491	4.22
736	350	2421	3.92	2202	4.99	2371	4.17
1004	350	2333	3.84	2092	5.00	2280	4.11
1956	350	2280	3.77	2043	4.99	2229	4.06
Bulk	350	1893	3.74	1879	4.99	1882	4.05
336	400	2802	4.11	2608	4.99	2751	4.29
484	400	2580	4.03	2374	5.00	2531	4.24
736	400	2461	3.96	2248	4.99	2411	4.20
1004	400	2383	3.89	2161	4.99	2331	4.15
1956	400	2331	3.80	2087	5.00	2279	4.08
Bulk	400	1897	3.79	1888	5.01	1893	4.07

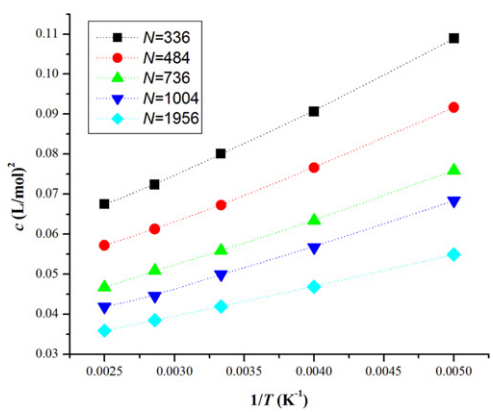

Fig. 4. Temperature dependence of the intercept, c, for different sizes of Ni nanoclusters which are obtained from fitting Eq. (4) (LIR II) to the simulation results.

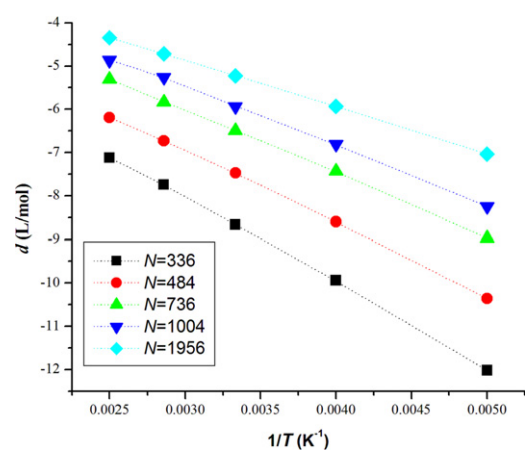

Fig. 5. The same as Fig. 4 for parameter d of LIR II.

nanoclusters. Also, the slopes in Figs. 4 and 5 are the largest (in magnitude) for the smallest nanocluster, which means that the parameters of the effective pair potential are the biggest for this nanocluster.

The size dependences of the parameters of LIR II are shown in Figs. 6 and 7, at five different temperatures. As may be expected, their absolute values become smaller for bigger nanoclusters, due to the smaller fraction of atoms on the surface.

The temperature dependences of the parameters of EOS III are presented in Figs. 8–10.

Each parameter of EOS III has two contributions: one is related to the thermal pressure and other to the internal pressure, and they have opposite signs [32]. Therefore, it is generally impossible to predict their signs. However, in the case of metals, f and e are related to the attraction and repulsion interaction of the effective pair potential, respectively. The term $g\rho^2$ is a small repulsion contribution, whose contribution is insignificant, except at extremely high pressures.

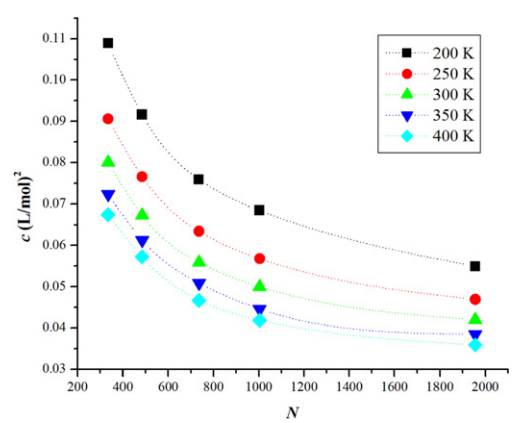

Fig. 6. Size dependence of parameter c of LIR II for different isotherms of a Ni nanocluster.

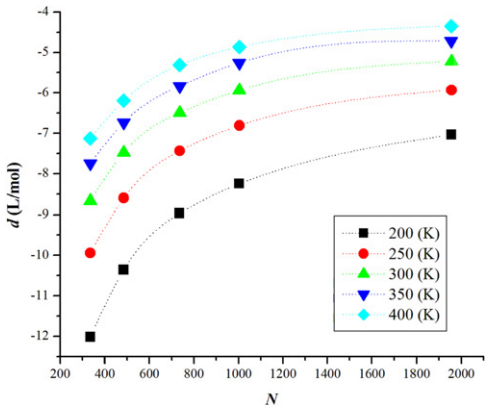

Fig. 7. The same as Fig. 6 for parameter *d* of LIR II.

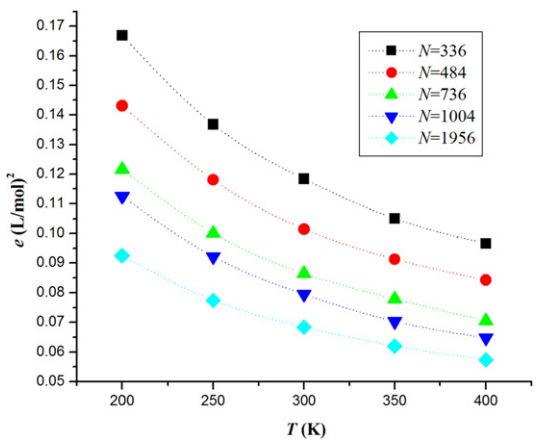

Fig. 8. Temperature dependence of parameter *e* for different Ni nanoclusters, obtained from fitting Eq. (5) (EOS III) to the simulation results.

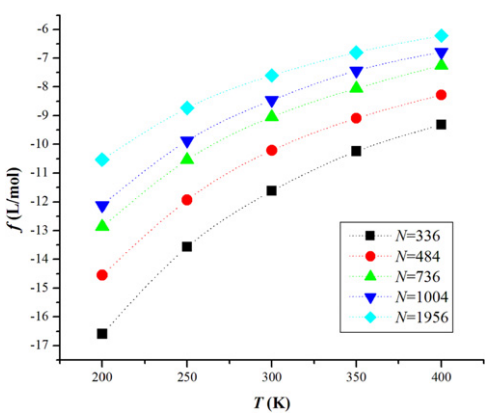

Fig. 9. The same as Fig. 8 for parameter *f*.

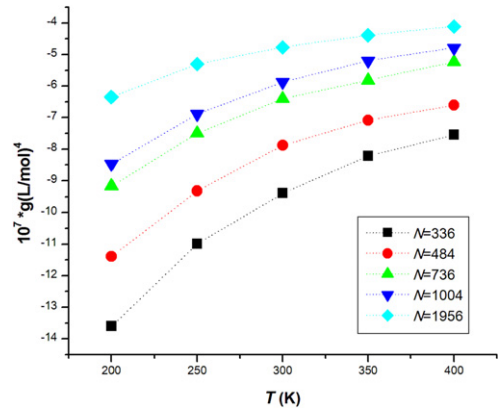

Fig. 10. The same as Fig. 8 for parameter *g*.

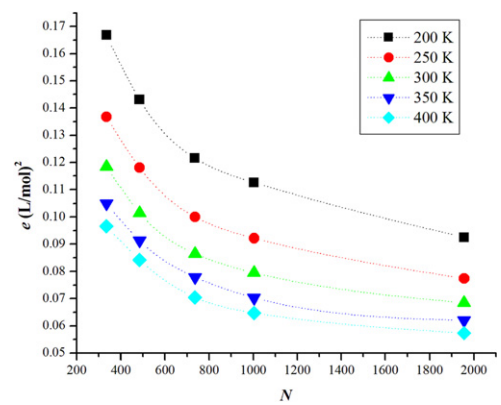

Fig. 11. Size dependence of parameter *e* for different isotherms of EOS III for a Ni nanocluster (the dotted lines are shown to guide the eye).

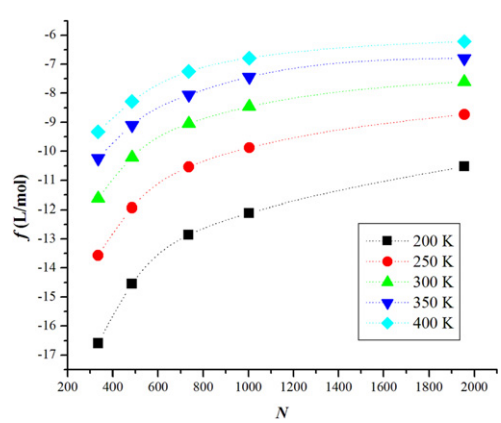

Fig. 12. The same as Fig. 11 for parameter *f* of EOS III.

The size dependences of the parameters of EOS III are shown in Figs. 11–13 at five different temperatures. As for the case of the parameters of LIR II, the size dependences of the *e*, *f*, and *g* parameters become smaller (in magnitude) for larger nanoclusters for the same reason given for LIR II.

Also, we have calculated the isobaric expansion coefficient for different cluster sizes at different temperatures via LIR II, assuming linear dependences for its parameters with $1/T$. The values of the isobaric expansion coefficient for each isotherm with given cluster sizes (and bulk) are summarized in Table 3. As shown in this table, an increase in isobaric expansion coefficient with decrease in number of particles can be observed. Since a smaller nanocluster has less binding energy per atom, on average, we may expect that it can be expanded more easily than a bigger cluster with temperature; hence, it has a larger value of the isothermal expansion coefficient, which is in accordance with the data of Table 3. Since the isothermal expansion coefficient is related to the lattice anharmonicity, we may conclude that it decreases with the cluster size, as shown in Table 3. Note that a smaller cluster has a larger fraction of surface atoms, which experience more asymmetric interactions, compared to the atoms in the bulk.

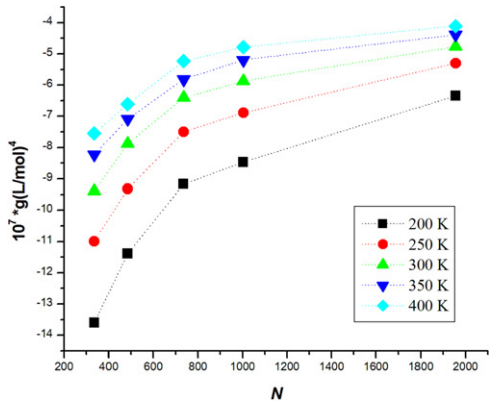

Fig. 13. The same as Fig. 11 for parameter g of EOS III.

Table 3
The calculated isobaric expansion coefficient at zero pressure for the bulk and nanoclusters of Ni with given sizes at five different temperatures, calculated from LIR II.

T (K)	N	Isobaric expansion coefficient $(K^{-1})*10^4$
200	336	2.71284
250	336	2.27412
300	336	2.11479
350	336	1.94861
400	336	1.85805
200	484	2.62027
250	484	2.25281
300	484	2.03625
350	484	1.86503
400	484	1.79033
200	736	2.47332
250	736	2.13094
300	736	1.93786
350	736	1.83855
400	736	1.68546
200	1004	2.19085
250	1004	1.90248
300	1004	1.75170
350	1004	1.58582
400	1004	1.57314
200	1956	1.73582
250	1956	1.57973
300	1956	1.45583
350	1956	1.38511
400	1956	1.29196
200	Bulk	0.178700
250	Bulk	0.160900
300	Bulk	0.146700
350	Bulk	0.134100
400	Bulk	0.125800

5. Conclusions

We have presented a method for applying pressure in the computer simulation of nanoparticles, using an ideal gas as the pressure medium. This method is especially suitable for finite systems. We have compared the accuracy of three EoSs of solids, namely the Linear Isotherm Regularity-II (LIR II), Birch–Murnaghan (BM), and EOS III, by fitting their expressions into the simulation data and also with zero-pressure quantities used as input data. Since the density range of our data is limited to less than 20% change, we have not been able to compare the predictive power of the three EoSs. However, one could do such a comparison if the density range is large enough. For instance, it was found that EOS III is very accurate even for very large pressure ranges [32].

The values of B_0 and B_0' for each isotherm with different cluster sizes are calculated via the EoSs, for which the results are summarized in Table 2. An increase in bulk modulus with decrease in number of particles of the cluster has been observed. As the cluster size decreases, proportionally more atoms are on the cluster surface. Surface atoms have less binding energy, compared to the bulk atoms; therefore, when the number of particles decreases, the compressibility is expected to decrease. Also, we have calculated the isobaric expansion coefficient for different cluster sizes at different temperatures via LIR II (see Table 3). An increase in isobaric expansion coefficient with decrease in number of particles has been observed, which may mean that the anharmonicity increases when the cluster size reduces. Also, a decrease in isobaric expansivity with increase in temperature has been found.

References

[1] D. Errandonea, B. Schwager, R. Ditz, C. Gessmann, R. Boehler, M. Ross, Phys. Rev. B 63 (2001) 132104.
[2] K.W. Katahara, M.H. Manghnani, E.S. Fisher, J. Phys. F: Met. Phys. 9 (1979) 773.
[3] R.G. McQueen, S.P. Marsh, J.W. Taylor, J.N. Fritz, W.J. Karter, in: R. Kinslow (Ed.), High Velocity Impact Phenomena, vol. 1, Academic, San Diego, CA, 1970, p. 294.
[4] J. Xiaogang, Z. Hanzao, C. Rongzhong, Z. Lei, Z. Quing, L. Jing, X. Lisong, AIP Conf. Proc. 429 (1998) 99.
[5] B. Chen, D. Penwell, M.B. Kruger, Solid State Commun. 115 (2000) 191.
[6] A. Kara, T.S. Rahman, Phys. Rev. Lett. 81 (1998) 1453.
[7] S. Rekhi, S.K. Saxena, R. Ahuja, B. Johanssan, J. Hu, J. Mater. Sci. 36 (2001) 4719.
[8] S.V. Raju, S.R. Kulkarni, S.K. Saxena, H.P. Liermann, S.V. Sinogeikin, Appl. Phys. Lett. 89 (2006) 261901.
[9] S.J. Zhao, K. Albe, H. Hahn, Scr. Mater. 55 (2006) 473.
[10] R. Martonak, C. Molteni, M. Parinello, Phys. Rev. Lett. 84 (2000) 682.
[11] R. Martonak, L. Colombo, C. Molteni, M. Parinello, J. Chem. Phys. 117 (2002) 11329.
[12] R. Martonak, C. Molteni, M. Parinello, Comput. Mater. Sci. 20 (2001) 293.
[13] N. Binggeli, J.R. Chelikowsky, Nature (London) 353 (1991) 344.
[14] B.J. Morgan, P.A. Madden, Nano Lett. 4 (2004) 1581.
[15] S. Kodiyalam, R.K. Kalia, H. Kikuchi, A. Nakano, F. Shimojo, P. Vashishta, Phys. Rev. Lett. 86 (2001) 55.
[16] S. Kodiyalam, R.K. Kalia, A. Nakano, P. Vashishta, Phys. Rev. Lett. 93 (2004) 203401.
[17] M. Grunwald, C. Dellago, Mol. Phys. 104 (2006) 3709.
[18] D.Y. Sun, X.G. Gong, J. Phys.: Condens. Matter 14 (2002) L487.
[19] Y.Y. Cheng, C.C. Lee, Nucl. Instrum. Methods Phys. Res. B 267 (2009) 1428.
[20] S.E. Baltazar, A.H. Romero, J.L. Rodriguez-Lopez, R Martonak, J. Phys.: Condens. Matter. 18 (2006) 9119.
[21] C. Bealing, G. Fugallo, R. Martonak, C. Molteni, Phys. Chem. Chem. Phys. 12 (2010) 8542.
[22] A.P. Sutton, J. Chen, Phil. Mag. Lett. 61 (1990) 139.
[23] Y. Qi, T. Cagin, Y. Kimura, W.A. Goddard III, Phys. Rev. B 59 (1999) 3527.
[24] S. Nose, J. Phys.: Condens. Matter. 2 (1990) 115.
[25] W. Smith, I.T. Todorov, Mol. Simul. 32 (2006) 935.
[26] P. Lazor, Ph.D. thesis, Uppsala University, 1993.
[27] P. Lazor, S.K. Saxena, Terra Nova 5 (1993) 363.
[28] F.D. Marnaghan, Proc. Natl. Acad. Sci. USA 30 (1944) 244.
[29] F. Birch, J. Geophys. Res. 57 (1952) 227.
[30] G.A. Parsafar, E.A. Mason, J. Phys. Chem. 97 (1993) 9048.
[31] M. Shokouhi, G.A. Parsafar, M.H. Dinpajooh, Fluid Phase Equilib. 271 (2008) 94.
[32] G.A. Parsafar, H.V. Spohr, G.N. Patey, J. Phys. Chem. B 113 (2009) 11977.
[33] E.O. Hall, Proc. Phys. Soc. London, Sect. B 64 (1951) 747.
[34] N.J. Petch, J. Iron Steel Inst., London 174 (1953) 25.
[35] R.W. Seigel, G.E. Fougere, in: G.C. Hadjipanayis, R.W. Seigel (Eds.), Nanophase Materials, vol. 260, Kluwer, Dordrecht, 1994, p. 233.
[36] A.H. Chokshi, A. Rosen, J. Karach, H. Gletter, Scr. Metall. 23 (1989) 1679.
[37] M.H. Ghatee, M. Bahadori, J. Phys. Chem. B 108 (2004) 4141.